JOURNAL OF AIRCRAFT
Vol. 31, No. 2, March–April 1994

Development of an Improved Model for Runback Water on Aircraft Surfaces

Kamel M. Al-Khalil*
National Research Council, Washington, D.C. 20418
and
Theo G. Keith Jr.† and Kenneth J. De Witt‡
University of Toledo, Toledo, Ohio 43606

A computer simulation for "running wet" and evaporative aircraft anti-icing systems is developed. The model is based on the analysis of the liquid water film which forms in the regions of direct impingement, and then breaks up near the impingement limits into rivulets. The wetness factor distribution resulting from the film breakup and the rivulet configuration on the surface are predicted using a stability analysis theory and the laws of mass and energy conservation. The solid structure is modeled as a multiple layer wall. The anti-icing system modeled is of the thermal type utilizing hot air and/or electrical heating elements embedded within the wall layers. Experimental observations revealing some of the basic physics of the water flow on the surface are presented. Detailed qualitative documentation of the tests are given. Several numerical examples are considered, and the effect of some of the involved parameters on the system performance are investigated.

Nomenclature

b = rivulet width at the base
C_p = pressure coefficient or specific heat
F = wetness factor
h_∞ = heat transfer coefficient between the freestream and the outer surface of the wall
LWC = liquid water content, g/m^3
M = Mach number
MVD = mean volume droplet diameter, μm
m = runback water mass flow rate
q = rate of heat transfer per unit area
T = temperature
β = droplet collection efficiency
δ = film/rivulet maximum thickness
θ = rivulet contact angle with the solid surface
λ = ratio of rivulet width to wetness factor, or distance between two adjacent surface streamlines

Subscripts
ai = anti-ice
f = liquid film, or rectangular film equivalent to a rivulet
r = rivulet
∞ = freestream

I. Introduction

THE problem of aircraft icing has been a subject of concern for the past few decades. The effects of ice accretion on critical surfaces are detrimental to the flight safety as well as to the aircraft aerodynamic performance. Consequently, accurate modeling and extensive study of the icing process are necessary. Two general methods of ice protection have been adopted: 1) de-icing methods for the intermittent removal of ice buildup by destruction of the bond between the ice and the surface; and 2) anti-icing methods for the prevention of ice formation on critical surfaces such as engine inlet nacelles.

The availability of high-speed digital computers has promoted the use of numerical techniques and the development of computer codes to design and analyze ice protection systems. It is felt that the latter, when validated and a sufficient confidence level in the results is reached, can minimize the cost associated with the required experimental testing. It would also provide a tool that is at least capable of predicting preliminary meaningful results.

Most studies related to aircraft icing have been committed to the prediction of ice shapes and the determination of their detrimental effects on aerodynamic performance of the aircraft components. Currently, research in running wet anti-icing systems is quite basic, and runback water is treated in a rather primitive manner. The NASA Lewis Research Center has been a major contributor in conducting and sponsoring studies related to computer modeling of aircraft icing processes, as well as experimental testing in its Icing Research Tunnel (IRT). As a result, LEWICE,[1] an ice accretion prediction code, was developed for unprotected airfoil surfaces. The approach used in the modeling consists of performing mass and energy balances on the surface water. The wetness factor issue is ignored, and the runback water is assumed to wet the entire surface at a particular location. Consequently, the amount of heat required to anti-ice the surface is largely underestimated by the LEWICE code, which was developed for the main purpose of predicting ice shapes.

Several investigators have produced different versions of LEWICE in order to improve it. To name a few, Cebeci et al.[2] modified the flowfield calculation module of the code to avoid the problem of multiple stagnation points. Yamaguchi et al.[3] proposed a multizone roughness model: a zone of uniform water film in the stagnation region, a rough zone of stationary water beads, and lastly, a zone where surface water run back as rivulets.[4] The runback water was recently modeled by Al-Khalil et al.[5–7] by incorporating a rivulet model. This model is discussed in the following sections.

II. Mathematical Model

The runback model utilized herein is based on a two-dimensional mathematical formulation. The surface water and

Presented as Paper 92-0042 at the AIAA 30th Aerospace Sciences Meeting, Reno, NV, Jan. 6–9, 1992; received Feb. 19, 1992; revision received Jan. 7, 1993; accepted for publication Jan. 8, 1993.

*NRC Research Associate, NASA Lewis Research Center.
†Professor, Mechanical Engineering Department.
‡Professor, Chemical Engineering Department.

the solid structure temperatures vary across their thicknesses and in the flow direction along a streamline on the surface. Spanwise temperature dependence is assumed to be negligible. However, the latter is accounted for by performing energy balances on control volumes whose spanwise widths extend between two adjacent streamlines on the aircraft surface. The latter are determined from the flowfield solution.

A. Runback Water

Supercooled liquid water droplets may exist in clouds at atmospheric temperatures much below freezing. While flying through a cloud of water droplets, leading aircraft surfaces strike a portion of the suspended liquid particles. The rate of impinging water is, however, relatively small. Due to this fact, and the aerodynamic forces, a very shallow water film forms on the skin surface and runs back to downstream regions. Consequently, the surface water behavior is controlled not only by aerodynamic and body forces, but also by surface tension forces and surface roughness.

In the direct impingement regions, i.e., in the neighborhood of the stagnation point, the water tends to wet the entire surface due to incoming droplets and due to water running back from upstream locations. However, near the impingement limits, the liquid film could become unstable due to surface tension forces which cause the surface water to coalesce into individual streams, referred to as rivulets, separated by dry areas. Similar effects have been experimentally observed in the direct impingement regions where water beads, initially stationary, formed. However, the spaces between the beads were still wetted by a very thin liquid layer. This validates the assumption of a totally wet surface in the direct impingement regions.

A detailed study on the hydrodynamics and a stability analysis of surface water are presented in Ref. 5. The film/rivulet flow in the streamwise direction is caused by a shear force acting at the liquid-air interface. The latter force is obtained from the results of the skin friction factor computed from viscous aerodynamic calculations of the flowfield.

A rectangular film model was chosen only to mathematically represent the heat transfer process in a rivulet as shown in Fig. 1. This model was found appropriate to the current problem for various reasons.[6] The criteria used for the new runback water configuration are as follows:

1) The wetness factor is preserved, i.e., the width of a rectangular film is equal to that of the corresponding actual rivulet.

2) The law of mass conservation requires equal mass flow rates in a rivulet and its equivalent rectangular film. This criterion is used to compute the rectangular film thickness δ_f, or simply, the film thickness.

3) Mass loss due to evaporation is associated with a decrease in the rivulet size, i.e., its radius and, consequently, its base width that is also equal to the rectangular film width. This criterion enables one to update the value of the wetness factor.

An area correction factor was used to account for the area differences between an actual rivulet and the rectangular film models through which heat exchange with the ambient occurs. This factor is defined as the ratio of the rivulet free surface area to the upper surface area of the corresponding rectangular film. This factor, which may be shown to be $\theta/\sin\theta$, is less than 1.1 for contact angles smaller than 42 deg, and is unity for uniform film flow.

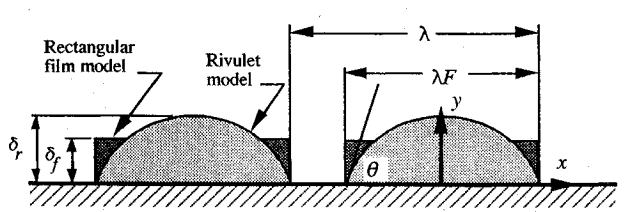

Fig. 1 Rivulet and equivalent rectangular film models.

The principal objective of the current study is to provide a tool to analyze and predict the performance of anti-icing systems. In such applications, the worse case normally occurs at equilibrium state conditions. Consequently, the mathematical formulation of the heat transfer process is based on the steady-state energy equations. The unsteady equations are more relevant to de-icing applications where prediction of ice shedding is a key aspect.

B. Anti-Ice Bleed Air

A widely used method for preventing ice formation is the hot air type system, due to its proven high reliability. In these systems, hot air is generally drawn from an intermediate- or high-stage compressor bleed port and ducted through passages to the leading edges of wings, empennages, engine nacelles, or other critical areas. Due to the complexity of the flow of the anti-icing air inside the irregular duct shapes and the uniqueness of each design, a generalized model requires the following assumptions:

1) The heating requirement by such a system is generally specified by the rate of hot air supply and its delivery temperature at the stagnation region.

2) The internal heat transfer coefficient distribution between the hot air and the inside surface of the structure is assumed to be known from previous experience or from experimental testing on the particular system in consideration.

3) The hot air temperature varies in the flow direction and is assumed to be lumped (uniformly averaged) in the transverse direction.

Since the anti-ice air temperature distribution depends on the solid wall temperature distribution which also depends on the runback water solutions, the energy equations of those three regions must be solved simultaneously.

C. Wall Structure

Based on the assumption that the wall temperature is dependent on the transverse and streamwise directions, an energy equation may be written for each layer in the composite structure. The temperature in the spanwise direction is assumed to be constant, but the variable width of the strips being analyzed in that direction is accounted for. This width is constant only in the case of a two-dimensional flow over a surface such as an airfoil.

The mathematical formulation allows a heating element to be modeled as one of the layers. The formulation also allows anti-icing to be achieved by means of a hot air system, electrical heating elements, or simply applying a specified heat flux at the wall. In addition, any combination of the latter is permitted. This type of formulation was chosen to give the flexibility of modeling different systems. The two conditions that must be satisfied at each solid-solid interface between the wall layers are continuity of temperature and heat flux normal to the interface. Similar conditions must be satisfied at the outer surface of the wall where heat is conducted to the runback water (in the wet regions), and convected to the ambient (in the dry regions).

III. Numerical Solutions

The required solutions are the temperature distributions in the anti-ice hot air, the solid structure, and the runback water. In addition, the surface water mass flow rate and the film/rivulets configuration must be determined. A simultaneous solution must be carried in the three regions: 1) runback water, 2) solid structure, and 3) anti-ice bleed air. This may not be accomplished in a single step due to the dependency of some boundary conditions of a particular region on the final solution in the adjacent region. This suggests the use of an iterative type of numerical solution between the three regions. Details of the numerical solution procedure are presented in Ref. 7. However, a brief description of the methods used are given in the following paragraphs.

A fully implicit method was used to numerically solve the runback water energy equation because of its positive stability properties. Backwards differencing in the streamwise direction, and central differencing in the transverse direction were employed.

The numerical solution requires the discretization of the water domain into grid points. Across the liquid layer thickness, equal spacing between the grid points was used. Along the flow direction, two zones were selected: 1) direct impingement region, and 2) downstream region. A constant grid spacing was chosen in each zone, but it is much smaller in the direct impingement region to accommodate for the rapidly changing variables due to the impinging water droplets and the flowfield characteristics.

The current model was specifically developed for anti-icing applications where at least the minimum heat required to keep the surface water from freezing is supplied to the surface. This is because a two-dimensional phase-change model was found to be inappropriate since freezing will normally start at the liquid-air interface, which creates a problem in modeling the flow characteristics of the unfrozen water. However, since the temperature drop across the film thickness is small, the temperature may be assumed to be uniform across the layer. Therefore, when a freezing (or lower) temperature is attained during the calculation process, an alternate method is used. This consists of performing a macroscopic energy balance on the surface water to obtain the freezing fraction, such as done in the LEWICE code.[1] Nevertheless, the rivulet configuration and its prediction remain the same. This enables one to predict the amount and location of ice accumulation during a specified period of exposure time.

The governing energy equation of the anti-ice bleed air is a first-order ordinary differential equation (ODE). Due to the arbitrary distribution of the heat transfer coefficient and the wall temperature at the inside surface of the solid structure, a numerical technique must be used to solve the latter equation. A forward finite difference scheme is only first-order accurate. A more accurate and widely used technique for solving ODEs is the fourth-order Runge-Kutta method. Knowing the temperature distribution in the wall, from the most recent iteration, the latter method is used to predict or update the hot air temperature distribution in the cowl. The result is subsequently used in the wall temperature solution at the next iteration.

In cases where anti-icing is achieved by means other than the hot air type, the solution of the hot air energy equation using the aforementioned technique is avoided. Instead, the air in the cowl is considered to be stagnant and at a prescribed temperature. Also, when the internal heat transfer coefficient is zero (i.e., insulated inner surfaces), there is no need to solve the latter equation since the result is a constant air temperature which does not affect the wall temperature, and consequently, the runback water temperature.

As to the layers in the wall structure, a control volume approach was chosen due to its accurate energy conservation properties. Difference equations are derived by performing an energy balance on each control volume corresponding to a particular node. The control surfaces of each control volume are halfway between the corresponding node and its adjacent surrounding nodes. There exist 11 types of nodes in the wall structure. Energy balance equations for each node type were presented in Ref. 7, as well as the details of the iterative solution procedure between the regions of interest.

IV. Experimental and Physical Observations

Important observations were made during recent experimental tests conducted in the NASA Lewis IRT by Cox & Company. The main purpose of the tests was to validate the performance of some advanced electrothermal anti-icing systems. Nevertheless, this provided a good opportunity to verify the basis of the rivulet runback physical model by observing the behavior of water after impinging on the surface.

The physical observations were recorded using several photographic instruments. These included still photography as well as motion pictures, using a 35-mm SLR camera and a S-VHS camcorder, respectively. Close-ups were taken using high magnification zoom lenses along with extension tubes on most of the photographic equipment. In addition, the Kodak EktaPro 1000, a high-speed imaging system, was used to capture the moving water drops and streams on the surface. The EktaPro is equipped with an image intensifier which acts as an electronic shutter and light amplifier. This makes it possible to capture events in a low light environment. Its processor is also equipped with two video output jacks for transferring images to other devices. Although it is capable of capturing up to 1000 full frames/s, a speed of 250 frames/s was found to be adequate for this purpose.

The physics of the surface water flow will only be qualitatively presented here since the reduction of the acquired data has not yet been completed. The following discussion is restricted to cases where at least the minimum heating requirement to keep the runback water from freezing was supplied to the surface, unless otherwise mentioned.

In the first series of tests, the outer skin of the model being tested, the aft RCS Vane of the B-1B engine inlet, was made of stainless steel with a very smooth surface. The solid wall was composed of several layers within which electrical heating elements were installed for the purpose of anti-icing. The system employs a multichannel control module to control the amount of electrical current, and therefore, the local surface temperature, to each individual heating element.

The experiments were carried out at various ranges of airspeeds, air temperatures, and cloud conditions. In addition, the anti-icing system design provided a mechanism to yield a prescribed surface temperature to control the amount of runback water. A high degree of visual documentation was accomplished for the various test cases. Different surface water flow characteristics were observed and are discussed in the following.

Several anti-icing test cases were conducted. Observations showed that upstream of the location where rivulet formation started, the entire surface was totally wet. As will be discussed later, the location where the film breaks up into rivulets is related to the limits where the droplets impinge on the surface. One approach to obtain qualitative information on the impingement patterns is to accrete a thin layer of rime ice on the model. The limits of accreted ice should closely coincide with the limits of impingement. This technique was applied and the results suggested that the water film in the direct impingement regions broke up into rivulets at the impingement limits.

One phenomenon worth mentioning is the formation of runback water on the surface in the form of beads (macroscopic drops). In earlier experimental studies performed by Olsen and Walker,[8] close-up movies were taken of the ice accretion process near the stagnation line, within a total distance of approximately 1 cm. These observations showed that the surface water drops grow due to the coalescence of many microscopic cloud droplets impacting the surface. When the surface drops grow large enough, the aerodynamic forces overcome the surface adhesion forces, and the drops move downstream along the surface. As the drops move along the surface, they sweep other surface drops. Larger drops exist at the stagnation line due to the smaller aerodynamic forces. Also, larger drops form for lower airspeeds for the same reason.

The current study suggested that such phenomena occur when, for one reason, the amount of surface mass flow rate is small. This is true for the following cases: 1) a relatively thin leading-edge airfoil, 2) low cloud liquid water contents, and 3) low runback mass flow rates due to high evaporation rates caused by a large amount of heating supply at the stag-

nation region. However, in cases of large amounts of runback water, drops occasionally form and are swept back, thus establishing paths for continuous flow of rivulets. Another reason for the formation of water beads is the highly smooth solid surface which decreases the adhesion forces between the drops and the surface, consequently increasing the contact angle θ (Fig. 1).

Another situation was observed where water beads formed downstream of the impingement regions and "rolled" back downhill. Observations showed that this occurred only for a smooth surface condition for reasons similar to the ones mentioned above. This phenomenon was most obvious when the runback water temperature near the trailing edge of a rivulet approached freezing and the rivulet stopped flowing at that location. However, since liquid water is still flowing from upstream regions, a drop forms and progressively gets large enough (relatively fast) to be swept back along the surface due to aerodynamic forces. At this instant, many of the drops were noticed to turn to a milky white color as they rolled back, which suggests that they were beginning to freeze.

A second series of tests were conducted on the engine inlet cowling of the Apache AH-64A helicopter. The coating of the nacelle produced a surface that is equivalent to sand grain roughness. Microscopic surface roughening has the effect of driving the contact angle θ farther from 90 deg.[9] In other words, if θ is less than 90 deg on a smooth surface, which is the case for water on most solid surfaces, roughening the surface decreases θ due to the increase in the water to surface adhesion forces. Consequently, the wettability of the surface increases and the runback water bead formation is eliminated as was found in these series of tests.

In the latter series of tests, it was clearly shown that the direct impingement regions were fully covered with a continuous thin film of water, while at the limits of the impingement regions the surface water run back as rivulets. Once established at the initial moments of spraying, the rivulet structure essentially remained unchanged throughout the duration of the test. It was also noticed that the rivulets followed paths which should coincide with the surface streamlines. These paths were not parallel due to the three-dimensional geometry of the nacelle. This was clearly seen near the downstream regions and around the nacelle rounded corners where the wetness factor was reduced mainly due to the fact that surface streamlines were becoming more widely spaced.

A wettable surface is a desirable property in anti-icing applications for the following reasons: the anti-ice heat supplied to the surface is conducted to the water in the wet regions and convected to the ambient in the dry regions. The latter portion of heat transfer is considered as wasted energy. This is one of the reasons why a large portion of the heat distributed on the surface is concentrated near the leading edges where the surface is fully wet (wetness factor equals 1).

The maximum rivulet thickness δ_r is larger than the continuous film thickness at the location of breakup. Furthermore, when the contact angle increases, the wetness factor decreases and δ_r increases for the same mass flow rate. This induces three drawbacks:

1) A thicker film is equivalent to more insulation between the liquid-air interface and the heated solid surface.

2) The thicker the film is, the faster water particles near the liquid-air interface will move downstream, which diminishes the amount of heat received by those particles to keep them from freezing. In other words, the residence time of those particles decreases at the upstream regions, where the larger portion of heat is supplied.

3) A decrease in the wetness factor decreases the system efficiency as discussed above. But eventually, when attempting to evaporate the runback water, the wetness factor will be forced to decrease. Thus, advantage should be taken to evaporate as much as possible in the direct impingement regions.

Consequently, heating requirements for total evaporation of runback water are larger in the case of rivulet flow structure than in the case of a continuous film due to the drop in the wetness factor. Thus, higher surface and heater temperatures result which, if exceeded beyond the capabilities of the structure materials, may cause delamination of the layers and probably damage to the heaters. Therefore, an optimum design would be to keep the surface as wettable as possible. One way to accomplish this would be to use a coating on the skin that produces a microscopically rough surface. This could reduce the aircraft aerodynamic performance. However, if this technique is applied only to engine inlets and a few other critical areas, the decrease in the aerodynamic performance may be offset. Another possible way is to add "contaminants" or wetting agents to the surface to decrease the contact angle of the rivulets. However, these agents would have to be applied periodically.

Lastly, a case of de-icing revealed an important issue of concern regarding thermal de-icers. The ice protection system under experimentation was controlled in such a way to provide heating to the leading edge only during a de-icing session. Ice was allowed to accrete at the leading edge of the model for over 5 min, then the forward heaters were activated. After a few seconds the secondary ice buildup, such as "rime feathers" which develop aft of the main ice accretion, shed off the surface keeping a few small water drops which rapidly evaporated. However, a few moments later, melted water from the ice-skin interface started to appear and progressively build up, while the "ice cap" was still holding to the leading edge due to aerodynamic forces.

The sudden change in the airfoil shape at the limits of accreted ice induced a separation of the flowfield at those regions. The separation bubble prevented the melted water from flowing downstream, in fact, the reversed flow was continuously pushing the water upstream, and when sufficient water accumulated, drove the water up near the tip of the ice at the ice accretion limits. At these locations, aerodynamic forces caused the water to shed and impact downstream on the surface near the location where the flowfield reattaches. Water drops formed there and grew, and then run back as beads/rivulets. Some drops moved back upstream on the surface because they fell slightly short of the flow reattachment location. This phenomenon is similar to that occurring near the stagnation line of a clean airfoil, where larger drops formed near the stagnation, as previously described.

Some existing thermal de-icing system designs rely on heating the leading-edge regions only to shed the accreted ice. In these systems, freezing runback rivulets were observed on the surface. For this reason, heating the surface further downstream is strongly recommended for a cleaner ice protected surface. Consequently, most de-icers use cyclic heating which may not be limited to leading edges only.

V. Numerical Calculations and Discussion

Several example problems will be considered in order to demonstrate the code capabilities and to investigate the effect of some of the dominant parameters in the problem. The complete solution to the problem is resolved in three major steps: 1) flowfield calculations, including the viscous layer near the wall; 2) individual water droplet trajectory calculations using the velocities calculated in the previous step; and finally 3) the heat transfer calculations for the anti-ice hot air, the solid structure, and the surface water.

The flowfield around the airfoil must be calculated such that viscous effects near the wall are accounted for. This is accomplished with a potential flow solver which includes a boundary-layer model. On the other hand, it may be accomplished using a code that numerically solves the full or a simplified version of the Navier-Stokes equations. ARC2D, a "thin layer" Navier-Stokes solver developed at NASA Ames, was used for this purpose. It has been used lately for icing

studies at NASA Lewis, and was found to give satisfactory results for low angles of attack. The model is adequate for high Reynolds number, and for attached and mildly separated flows where the viscous terms associated with derivatives in the direction parallel to the body are negligible. ARC2D uses a Baldwin-Lomax turbulence model which is a conventional two-layer model. The output format from the code was tailored to the inputs requirements of the current heat transfer code.

Due to the effects of viscosity near the solid surfaces, large gradients of the variables exist in these regions. This requires a fine grid spacing in the directions normal to the rigid body which allows the flow solver to capture all the necessary details in those regions. This was accomplished using a hyperbolic grid generator to produce a C-type grid structure around an airfoil. The curvilinear body-fitted mesh was composed of (239 grid points along the surface) × (55 nodes in the nearly normal direction). This is illustrated in Fig. 2 for a NACA 0012 symmetric airfoil which will be used as the solid structure in the following examples. The chord length is assumed to be equal to 1 m.

The droplet trajectory and impingement module of LEWICE was used to generate the collection efficiency curves. The code was modified to read and interpolate for the flowfield velocities from the outputs generated by ARC2D. Minor modifications were also required for the code to handle viscous flows.

The ambient operating conditions used in the numerical calculations are: $T_\infty = -12°C$, and $P_\infty = 90.75$ kPa. The airfoil angle of attack with the freestream is taken to be zero. This should yield symmetric results since the airfoil geometry is also symmetric. The flowfield around the airfoil was computed for two freestream speeds, $M_\infty = 0.3$ and $M_\infty = 0.4$. The resulting pressure and friction coefficients are illustrated in Figs. 3 and 4, respectively. The first coefficient may be used to calculate properties at the edge of the boundary layer, and the second is used to compute the wall shear layer stress

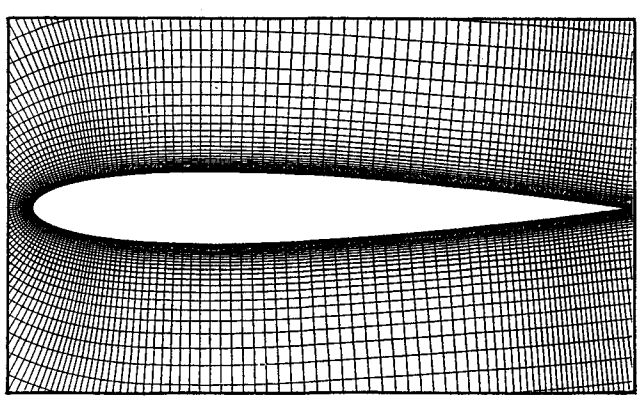

Fig. 2 Grid structure used in the flowfield calculations.

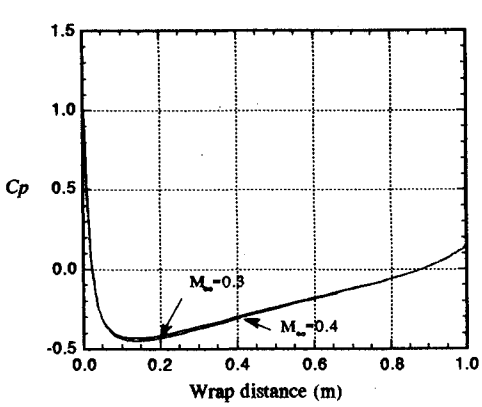

Fig. 3 Surface pressure coefficients.

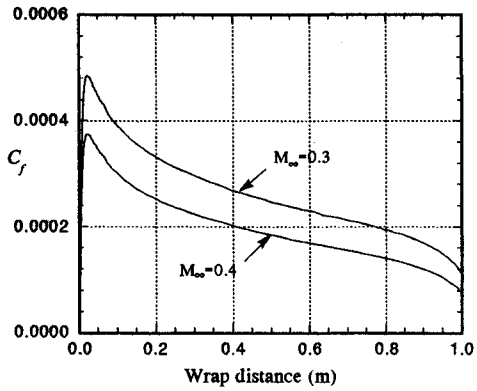

Fig. 4 Skin friction coefficients.

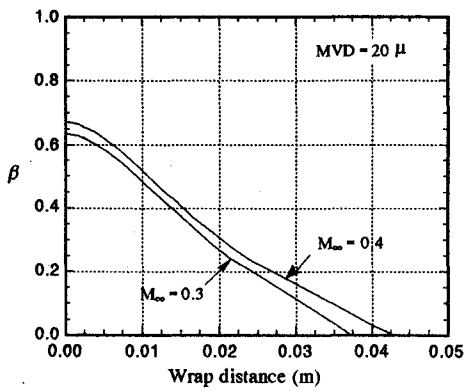

Fig. 5 Droplet collection efficiencies.

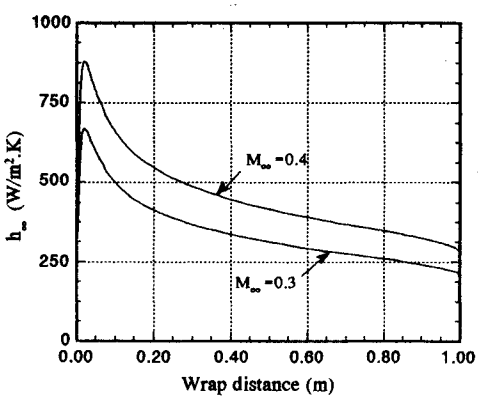

Fig. 6 Heat transfer coefficients.

that causes the surface water to flow to downstream regions. The particle trajectory was subsequently used to compute the local collection efficiencies. The cloud was assumed to be monodispersed with a droplet size of MVD = 20 μm. The results are shown in Fig. 5 for the two airspeeds.

The next step involves the heat transfer calculations using the flowfield and the trajectory solutions. The convective heat transfer coefficients between the airfoil surface and the ambient air were computed using a sand roughness factor of $k_s/c = 0.0002$.[1] The resulting distributions for both airspeeds considered are illustrated in Fig. 6. Obviously, higher airspeeds result in higher heat transfer coefficients. In all the calculations that follow, a contact angle of $\theta = 40$ deg between the rivulets and the solid surface was assumed when breakup of the film occurs. In reality, θ is mostly a function of the surface properties.

The stability analysis presented in Refs. 5 and 6 revealed that the film of water in the direct impingement regions is always unstable. In other words, the actual film thickness calculated in many cases is always smaller than the critical

value below which the film is unstable, and must break up. This is due to the relatively small rates of water impingement on aircraft surfaces in applications related to ice protection. This is what causes the formation of water drops in the direct impingement regions rather than a uniform film. These drops are initially stationary, but are swept back by aerodynamic forces when sufficiently large, as discussed earlier. Nevertheless, the impinging microscopic droplets continuously tend to wet the entire surface in the direct impingement regions by filling the gaps between the macroscopic droplets. However, near the impingement limits, the film must break up into rivulets due to the coalescence of water drops caused by surface tension. This phenomenon was revealed in the experimental studies discussed earlier.

Breakup of the film into rivulets was based on three criteria applied at the location of breakup: 1) mass flow rates are equal between the film and the rivulets; 2) the total mechanical energies (kinetic and surface tension) are also equal between the two; and 3) the total mechanical energy of the rivulets is minimum with respect to the spacing between the rivulets. These conditions yield the value of the critical film thickness, the rivulets size δ_r, and the spacing between the rivulets or the wetness factor F. However, as discussed above, the actual film thickness in most cases considered is much smaller than the critical film thickness. Thus, the results of δ_r and F are only valid for the case where the film thickness is equal to the critical value. Therefore, the first two criteria are used,[6] i.e., mass and total mechanical energy balances, and in most cases the value of F was overpredicted ($F \sim 0.5$–0.75), as compared to the experimental observations ($F \sim 0.3$–0.4). The latter values are actually very close to those predicted by the stability analysis ($F \sim 0.32$–0.39 for angles of $\theta \sim 10$–70 deg), as predicted in Ref. 5.

In regards to the above observations, the value of F is assumed to fall in the range of 0.3–0.4 at breakup, and the corresponding size of rivulets is obtained from the mass balance criterion. To develop an idea on the relative size of rivulets from the numerical calculations using this fact, Figs. 7 and 8 may be examined. These plots were obtained assuming LWC = 1.0 g/m^3, and a uniform heat flux q_{ai} = 19.4 W/in.^{2} is applied to the surface of the NACA 0012 airfoil. The rivulet width shown is approximately 0.6 mm for the range of F = 0.3–0.4, which generally agrees with preliminary measurements on the experimental observations. Therefore, a nominal value of F = 0.35 will be assumed in the rest of the numerical calculations. However, let's first examine the effect of the initial estimate of F on the results.

Figures 9–11 illustrate the effect of the initial estimate of the wetness factor on the wetness factor, the runback mass flow rate, and the runback average temperature distributions, respectively. The operating conditions are as shown on the plots. A larger initial value of F implies a larger heat and mass loss from the runback to the ambient due to the increased

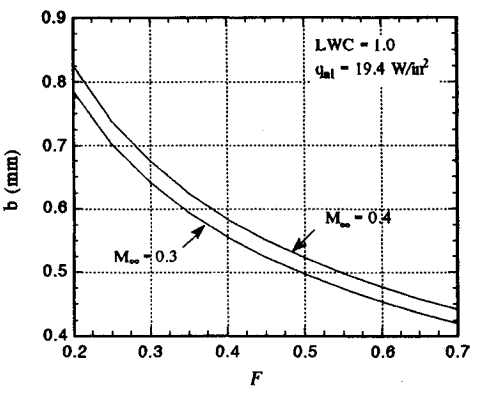

Fig. 7 Rivulet width at breakup as function of estimated wetness factor.

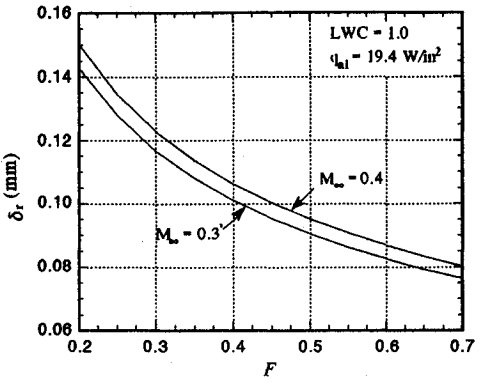

Fig. 8 Rivulet height at breakup as function of estimated wetness factor.

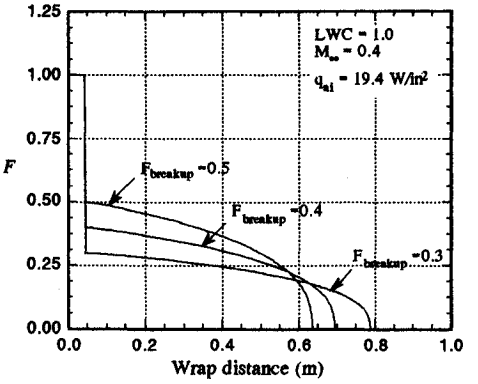

Fig. 9 Effect of the initial estimate of F on the wetness factor distribution.

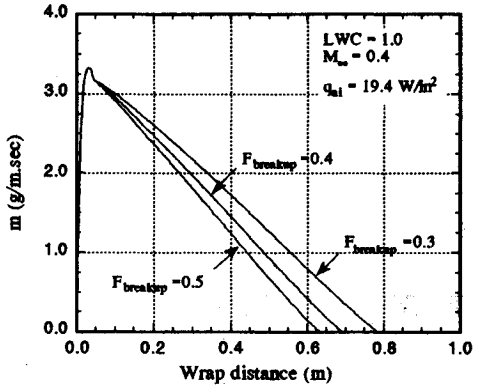

Fig. 10 Effect of the initial estimate of F on runback flow rate distribution.

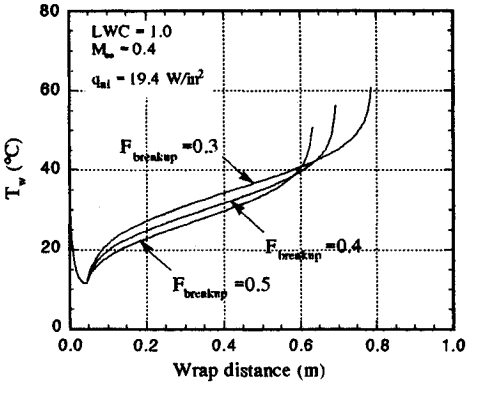

Fig. 11 Effect of the initial estimate of F on runback temperature distribution.

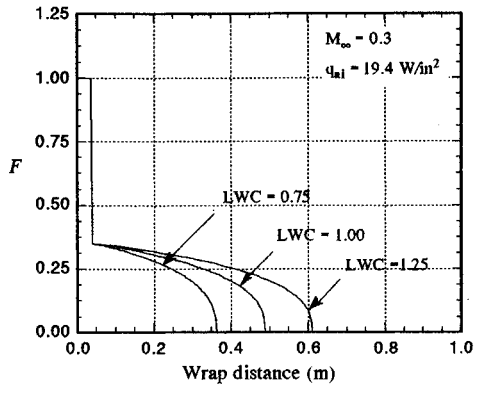

Fig. 12 Effect of LWC on the wetness factor distribution.

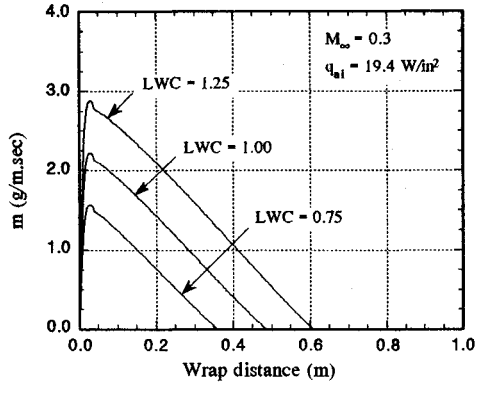

Fig. 13 Effect of LWC on the runback flow rate distribution.

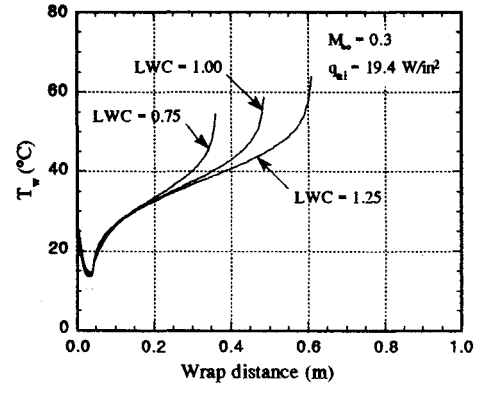

Fig. 14 Effect of LWC on the runback average temperature distribution.

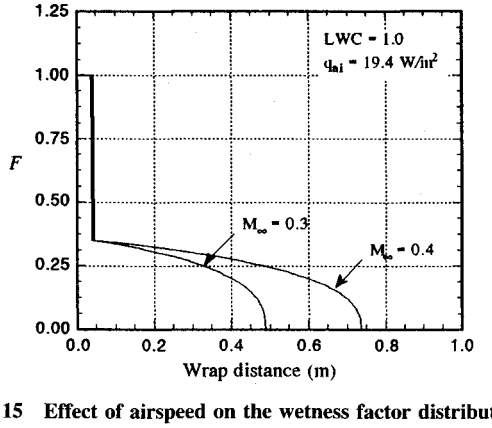

Fig. 15 Effect of airspeed on the wetness factor distribution.

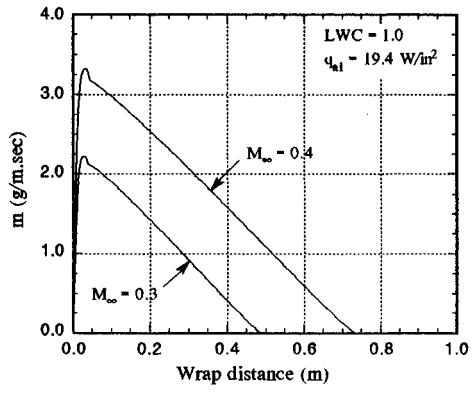

Fig. 16 Effect of airspeed on the runback flow rate distribution.

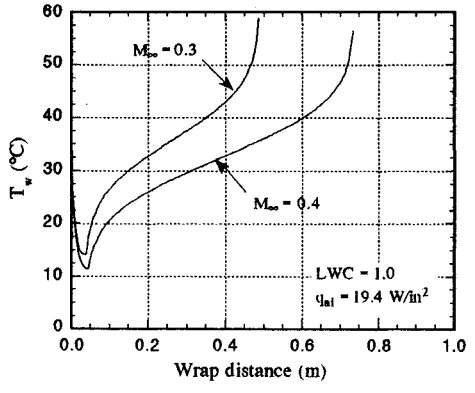

Fig. 17 Effect of airspeed on the runback average temperature distribution.

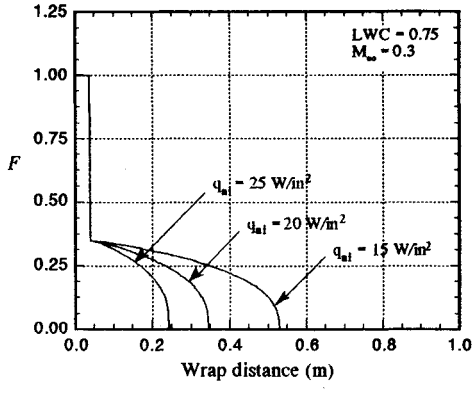

Fig. 18 Effect of q_{ai} on the wetness factor distribution.

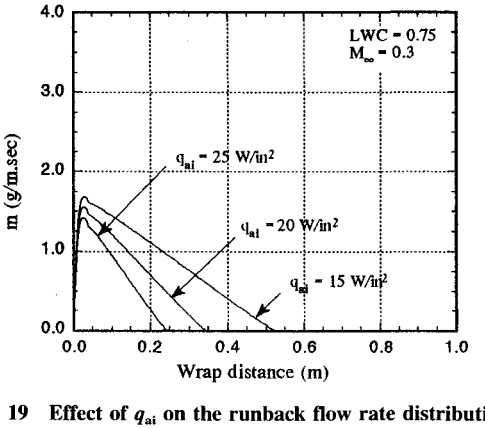

Fig. 19 Effect of q_{ai} on the runback flow rate distribution.

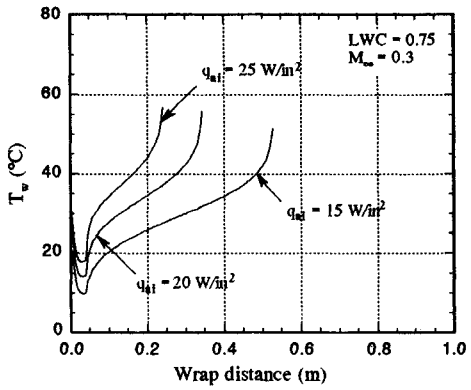

Fig. 20 Effect of q_{ai} on the runback average temperature distribution.

area, as illustrated in these figures. Therefore, at some location downstream, the wetness factor corresponding to the case of the larger initial value of F will decrease below that of the other cases due to the faster rate of mass loss. This proves the importance of the wetness factor variable and the need to appropriately represent it in the current numerical models.

The effects of the cloud liquid water content and the airspeed were also investigated. Figures 12–14 show the effects of LWC on the wetness factor, and the runback flow rate, and temperature distributions, respectively. The corresponding effects of M_∞ are illustrated in Figs. 15–17. The rate of water impingement is proportional to the product of LWC and M_∞. Thus, as expected, the liquid water runs back further downstream before totally evaporating in cases of higher LWC and/or M_∞. It is interesting to note that the runback mass flow rate decreases almost linearly (Figs. 10, 13, 16, and 19) with approximately a constant slope for varying LWC and M_∞, Figs. 13 and 16, and an increase in the slope for larger initial wetness factors and/or surface heat flux, Figs. 10 and 19.

The effects of the rate of heat applied to the surface on the wetness factor, the runback mass flow rate, and its average temperature distributions are illustrated in Figs. 18–20, respectively. Clearly, total evaporation of the runback water occurs at a shorter downstream location for a higher surface heat flux as expected. However, the total energy used for this purpose differs between the three cases shown in the figures. The total energy—the product of the heat flux q_{ai} and the distance of runback—increases with decreasing q_{ai}. This is because the amount of runback at the limit of impingement was reduced by applying more heat in the direct impingement region where the entire surface is wet and most of the heat is transferred to the water (in totally wet regions), rather than to the water and the ambient air (in partially wet regions). This suggests the use of a variable surface heat flux with the larger portion applied to leading edges, as discussed earlier. Nonetheless, the maximum tolerable temperature of the structure materials should not be exceeded.

VI. Concluding Remarks

The stability analysis developed earlier led to the conclusion that the liquid water film which forms in the regions of direct impingement will break up into rivulets near the impingement limits. The experimental observations agreed well with this conclusion. Also, preliminary comparisons between the numerical and experimental results of the relative size of rivulets were promising. In addition, the initial wetness factor at breakup fell in the range predicted by the stability analysis.

An efficient anti-icing system design may be achieved with a variable heat supply to the surface with the larger portion concentrated at the leading edges, such that the local structure temperature is still within a tolerable magnitude. This was due to the fact that the surface in these regions is entirely wet. The rate of heating requirements increases with increase in the freestream velocity and/or the liquid water content of the ambient air. Thus, a wettable surface is a desirable property in anti-icing applications, since more heat is transferred to the water to evaporate it and less heat is lost to the ambient through dry areas on the surface. A microscopically rough surface, for example, is more wettable than a very smooth surface. In most cases, heat should not only be restricted to leading edges.

Future work will include quantitative comparisons between the experimental and the numerical results to validate the current model. More detailed experimental studies may be required to achieve a complete data base on the behavior of surface water. This includes the size of drops and rivulets, the wetness factor distribution, and the effects of the ambient operating conditions, as well as the surface properties.

Acknowledgments

This work was done while K. M. Al-Khalil held a National Research Council Research Associateship at NASA Lewis Research Center. The sponsorship of these two organizations is gratefully acknowledged. Also, the cooperation of members of Cox & Company, Inc. with the experimental tests is appreciated.

References

[1]Ruff, G. A., and Berkowitz, B. M., "Users Manual for the NASA Lewis Ice Accretion Prediction Code (LEWICE)," NASA CR-185129, May 1990.

[2]Cebeci, T., Chen, H. H., and Alemdaroglu, N., "Fortified LEWICE with Viscous Effects," AIAA Paper 90-0754, Jan. 1990.

[3]Yamaguchi, K., Hansman, R., and Karmierczak, M., "Deterministic Multi-Zone Ice Accretion Modeling," AIAA Paper 91-0265, Jan. 1991.

[4]Hansman, R. J., Yamaguchi, K., Berkowitz, B., and Potapczuk, M., "Modeling of Surface Roughness Effects on Glaze Ice Accretion," AIAA Paper 89-0734, Jan. 1989.

[5]Al-Khalil, K. M., Keith, T. G., and De Witt, K. J., "Development of an Anti-Icing Runback Model," AIAA Paper 90-0759, Jan. 1990.

[6]Al-Khalil, K. M., Keith, T. G., and De Witt, K. J., "Further Development of an Anti-Icing Runback Model," AIAA Paper 91-0266, Jan. 1991.

[7]Al-Khalil, K. M., Keith, T. G., and De Witt, K. J., "Numerical Modeling of Runback Water on Ice Protected Aircraft Surfaces," Fifth Symposium on Numerical and Physical Aspects of Aerodynamic Flows, Long Beach, CA, Jan. 13–15, 1992.

[8]Olsen, W., and Walker, E., "Experimental Evidence for Modifying the Current Physical Model for Ice Accretion on Aircraft Surfaces," NASA TM-87184, May 1986.

[9]Davies, J. T., and Rideal, E. K., *Interfacial Phenomena*, 2nd ed., Academic Press, New York, 1963.